Dyes and Pigments 91 (2011) 248–257

Contents lists available at ScienceDirect

Dyes and Pigments

journal homepage: www.elsevier.com/locate/dyepig

Review

Computational study of the one- and two-photon absorption properties of macrocyclic thiophene derivatives

Shuang Huang [a], Ai-Min Ren [a,*], Lu-Yi Zou [a], Yang Zhao [a], Jing-Fu Guo [b,*], Ji-Kang Feng [a]

[a] State Key Laboratory of Theoretical and Computational Chemistry, Institute of Theoretical Chemistry, Jilin University, Changchun 130023, People's Republic of China
[b] School of Physics, Northeast Normal University, Changchun 130021, People's Republic of China

ARTICLE INFO

Article history:
Received 16 October 2010
Received in revised form
25 February 2011
Accepted 28 February 2011
Available online 8 March 2011

Keywords:
Macrocyclic thiophene derivatives
One-photon absorption
Two-photon absorption
TPA cross-section
Electronic structure
ZINDO method

ABSTRACT

The geometrical structure, electronic structure, one-photon and two-photon absorption properties of a series of macrocyclic thiophene derivatives C[3T_DA]$_n$ (n = 2–5) have been studied using density functional theory (DFT) and Zerner's intermediate neglect of differential overlap (ZINDO) methods theoretically. The results showed that the range of $\lambda^{(1)}_{max}$s is 390–470 nm and $\lambda^{(2)}_{max}$s is 640–670 nm, while, both $\lambda^{(1)}_{max}$ and $\lambda^{(2)}_{max}$ gradually enlarge as increasing the number of the C[3T_DA] unit. And C[3T_DA]$_n$ compounds exhibited large TPA cross-section (δ_{max}), and the factors influencing on the δ_{max} values were analyzed in detail. Transition dipole moments $\boldsymbol{M}_{0k}$ and $\boldsymbol{M}_{kn}$ play important roles on δ_{max}. Both π-electron number (N_e) and the product of oscillator strengths from ground state to mediate state (f_{0k}) and from mediate state to final state (f_{kn}) are in proportion to δ_{max}. Moreover, δ_{max} linearly depends on the static second-order nonlinear optical susceptibilities (β_0).

1. Introduction

With the development of organic conjugation molecules in recent years, new nonlinear optical materials are under considerable attention due to their potential applications in many different fields such as chemistry, photonic, and biological imaging [1–3]. Two-photon absorption (TPA) as a nonlinear optical (NLO) phenomenon has attracted increasing interest since 1931 [4]. TPA properties of organic materials exhibit bright future for many advanced applications such as two-photon imaging microscopy [5], photodynamic therapy [6], optically power limiting [7], three-dimensional (3D)-microfabrication [8], optical data storage [9], two-photon laser scanning fluorescence imaging [5,10,11] and so on. The development of two-photon technology depends largely on the success of synthesizing new material molecules with large TPA cross-section at desirable wavelengths. But until now, the practical TPA materials are still limited. The reason for this phenomenon is the structure–property relationship remains unclear. Moreover, exploration and research of new materials with large TPA cross-section and applicable in practice are urgent. So the study of the relationship between molecular structure and the TPA cross-section becomes quite important.

Based on the coherent interactions in multichromophore systems, strong enhancement of the TPA effect was possible [12]. In order to better understand the relationship between structure and property for the molecules with large TPA cross-section, a numerous of organic molecules have been investigated experimentally and theoretically [13–15]. The majority of the reports have concentrated on linear and branched architectures. As regards particular structures, the incorporation of heterocyclic rings has shown good TPA properties [16–18].

The current focus is to make well-defined π-conjugated macrocycles as modular building blocks for the programmed assembly on new molecular materials [19]. Compared with usual linear π-conjugated oligomers and polymers, if the macrocyclic systems are sufficiently stable and large, novel perspectives and properties will arise.

To best of our knowledge, some electronic structure calculations of thiophene-based systems have been investigated previously [20,21]. However, nonlinear optical properties of thiophenes in circular geometries other than linear chromophores have not been explored in detail. For example, macrocyclic thiophenes with relatively large cavities bearing good TPA properties and collective excitations have not been investigated. Linear thiophene oligomers have attracted considerable attention for their possible applications in light-emitting diodes, lasers, field-effect transistors, photovoltaic cells [22] and molecular nanowires [23] as a result of their excellent electron and energy transfer properties, and well π-conjugated

* Corresponding authors. Liutiao Road 2#, Changchun, People's Republic of China.
E-mail addresses: aimin_ren@yahoo.com (A.-M. Ren), guojf217@nenu.edu.cn (J.-F. Guo).

0143-7208/$ – see front matter © 2011 Elsevier Ltd. All rights reserved.
doi:10.1016/j.dyepig.2011.02.005

structures. On the other hand, the interesting properties of annular thiophene compounds are needed to further study.

As reported by Theodore Goodson III et al. [24], they have successfully synthesized a series of fully π-conjugated macrocyclic thiophene derivatives C[3T_DA]$_n$ (n = 2–5), whose main body consists of trithiophene and connected by diacetylene as a bridge. It increases π-conjugated extent through increasing the number of building blocks in the macrocycle. And some excellent properties were reported on one-photon absorption (OPA) [25,26]. About fluorescence emission, TPA cross-section, fluorescence quantum yield and lifetime were also examined by experiment [24,27]. While the research of the second-order nonlinear optical properties indicates C[3T_DA]$_n$ have large static second-order nonlinear optical coefficients (β_0) [25]. But the systematic theoretical study of relationship between structure and TPA property still has not been carried out. With this in mind, some new insights on the electronic structure of the macrocyclic thiophene derivatives depicted in Fig. 1 will be provided by OPA, TPA and TPA cross-section calculations using DFT and ZINDO program based on their stable physical and chemical properties in this work. The effect of the π-electronic delocalization of ring shape, macrocyclic dimension, transition dipole moment and oscillator strength, and their effects on TPA cross-section will be investigated. Combining the frontier molecular orbitals of studied molecules, we will make an effort to further explore the relationship between intramolecular charge transfer (ICT) and TPA cross-section, and the special relationship between TPA cross-section and static second-order nonlinear optical coefficient.

2. Theoretical methodology

The TPA process corresponds to the simultaneous absorption of two photons. The TPA efficiency of an organic molecule, at optical frequency $\omega/2\pi$, can be characterized by the TPA cross-section $\boldsymbol{\delta}(\omega)$. It can be directly related to the imaginary part of the third-order polarizability $\gamma\,(-\omega;\,\omega,\,\omega,\,-\omega)$ [28], as shown in Eq. (1):

$$\delta(\omega) = \frac{3(\hbar\omega)^2}{2n^2c^2\varepsilon_0\hbar}L^4\mathrm{Im}[\gamma(-\omega;\omega,-\omega,\omega)] \tag{1}$$

where

$\gamma\,(-\omega;\,\omega,\,\omega,\,-\omega)$ is the third-order polarizability;

$\hbar\omega$ is the energy of incoming photons;

c is the speed of light;

ε_0 is the vacuum electric permittivity;

n denotes the refractive index of the medium, and L corresponds to the local-field factor. In the calculations presented here, n and L are set to 1 because of isolated molecules in the vacuum.

The sum-over-states (SOS) expression to evaluate the components of the second hyperpolarizability $\gamma_{\alpha\beta\gamma\delta}$, can be deduced using perturbation theory. By considering a Taylor expansion of energy with respect to the applied field, the $\gamma_{\alpha\beta\gamma\delta}$ Cartesian components are given [29,30].

$$\begin{aligned}\gamma_{\alpha\beta\gamma\delta}(-\omega_\sigma;\omega_1,\omega_2,\omega_3) = {}& \hbar^{-3}\sum P_{1,2,3}\\ &\left(\sum_K{}'\sum_L{}'\sum_M{}'\left(\begin{array}{l}\dfrac{\langle 0|\mu_\alpha|K\rangle\langle K|\overline{\mu_\beta}|L\rangle\langle L|\overline{\mu_\gamma}|M\rangle\langle M|\mu_\delta|0\rangle}{(\omega_K-i\Gamma_K-\omega_\sigma)(\omega_L-i\Gamma_L-\omega_2-\omega_3)(\omega_M-i\Gamma_M-\omega_3)}\\ +\dfrac{\langle 0|\mu_\beta|K\rangle\langle K|\overline{\mu_\alpha}|L\rangle\langle L|\overline{\mu_\gamma}|M\rangle\langle M|\mu_\delta|0\rangle}{(\omega_K+i\Gamma_K+\omega_1)(\omega_L-i\Gamma_L-\omega_2-\omega_3)(\omega_M-i\Gamma_M-\omega_3)}\\ +\dfrac{\langle 0|\mu_\beta|K\rangle\langle K|\overline{\mu_\gamma}|L\rangle\langle L|\overline{\mu_\alpha}|M\rangle\langle M|\mu_\delta|0\rangle}{(\omega_K+i\Gamma_K+\omega_1)(\omega_L+i\Gamma_L+\omega_1+\omega_2)(\omega_M-i\Gamma_M-\omega_3)}\\ +\dfrac{\langle 0|\mu_\beta|K\rangle\langle K|\overline{\mu_\gamma}|L\rangle\langle L|\overline{\mu_\delta}|M\rangle\langle M|\mu_\alpha|0\rangle}{(\omega_K+i\Gamma_K+\omega_1)(\omega_L+i\Gamma_L+\omega_1+\omega_2)(\omega_M+i\Gamma_M+\omega_\sigma)}\end{array}\right)\\ &-\sum_K{}'\sum_L{}'\left(\begin{array}{l}\dfrac{\langle 0|\mu_\alpha|K\rangle\langle K|\mu_\beta|0\rangle\langle 0|\mu_\gamma|L\rangle\langle L|\mu_\delta|0\rangle}{(\omega_K-i\Gamma_K-\omega_\delta)(\omega_K-i\Gamma_K-\omega_1)(\omega_L-i\Gamma_L-\omega_3)}\\ +\dfrac{\langle 0|\mu_\alpha|K\rangle\langle K|\mu_\beta|0\rangle\langle 0|\mu_\gamma|L\rangle\langle L|\mu_\delta|0\rangle}{(\omega_K-i\Gamma_K-\omega_1)(\omega_L+i\Gamma_L+\omega_2)(\omega_L-i\Gamma_L-\omega_3)}\\ +\dfrac{\langle 0|\mu_\beta|K\rangle\langle K|\mu_\alpha|0\rangle\langle 0|\mu_\gamma|L\rangle\langle L|\mu_\delta|0\rangle}{(\omega_K+i\Gamma_K+\omega_1)(\omega_K+i\Gamma_K+\omega_\delta)(\omega_L+i\Gamma_L+\omega_2)}\\ +\dfrac{\langle 0|\mu_\beta|K\rangle\langle K|\mu_\alpha|0\rangle\langle 0|\mu_\gamma|L\rangle\langle L|\mu_\delta|0\rangle}{(\omega_K+i\Gamma_K+\omega_1)(\omega_L+i\Gamma_L+\omega_2)(\omega_L-i\Gamma_L-\omega_3)}\end{array}\right)\end{aligned} \tag{2}$$

In the formula,

α, β, γ and δ refer to the molecular axes;

ω_1, ω_2 and ω_3 are optical frequencies;

$\omega_\sigma = \omega_1 + \omega_2 + \omega_3$ is the polarization response frequency;

$\sum P_{1,2,3}$ indicates a sum over the terms obtained by the six permutations of the pairs (ω_1/μ_β), (ω_2/μ_γ), and (ω_3/μ_δ);

K, L and M denote excited states, and 0 denotes the ground state;

$|K\rangle$ is an electronic wave function with energy $\hbar\omega_K$ relative to the ground electronic state;

μ_α is the αth ($= x, y, z$) component of the dipole operator, $\langle K|\overline{\mu_\alpha}|L\rangle = \langle K|\mu_\alpha|L\rangle - \langle 0|\mu_\alpha|0\rangle$; the primes on the summation over the electronic states indicate exclusion of the ground state.

Γ_K is the damping factor of excited state K, and in the present work, all damping factors Γ are set to 0.14 eV; this choice of damping factor is found to be reasonable on the basis of the comparison between the theoretically calculated and experimental TPA spectra.

To compare the calculated $\boldsymbol{\delta}$ value with the experimental value measured in solution, the orientationally averaged (isotropic) value of γ is evaluated, which is defined as

$$\langle\gamma\rangle = \frac{1}{15}\sum_{i,j}\left(\gamma_{iijj}+\gamma_{ijij}+\gamma_{ijji}\right), \quad i,j = x,y,z \tag{3}$$

whereafter $\langle\gamma\rangle$ is taken into Eq. (1), and then the TPA cross-section $\boldsymbol{\delta}$ is obtained.

Generally, the position and relative strength of the two-photon resonance are to be predicted using the following simplified form of the SOS expression (Eq. (4)) [31],

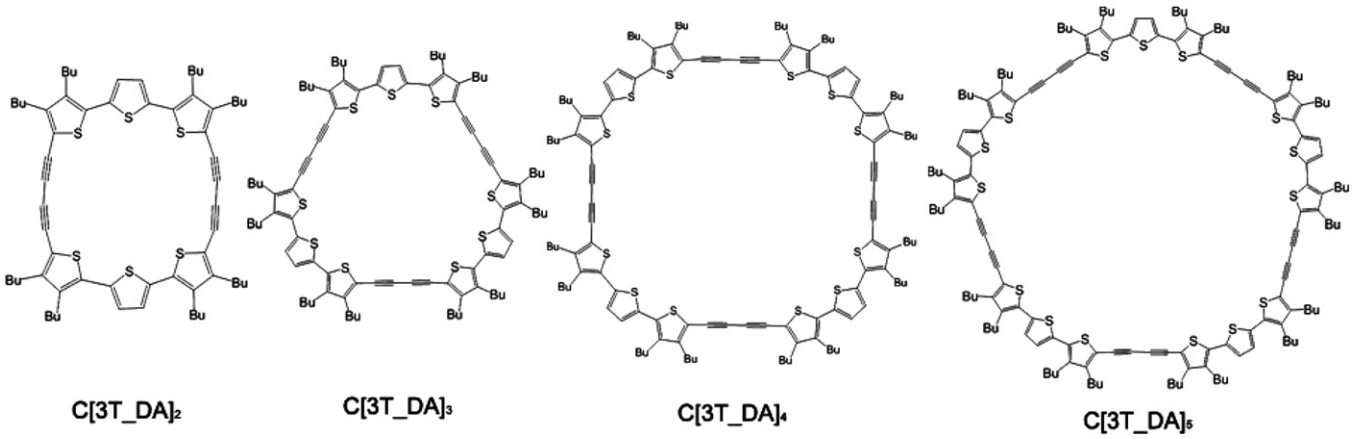

Fig. 1. Molecular structures of the studied molecules.

$$\delta \propto \frac{M_{0k}^2 M_{kn}^2}{(E_{0k} - E_{0n}/2)^2 \Gamma} + \frac{M_{0n}^2 \Delta\mu_{0n}^2}{(E_{0n}/2)^2 \Gamma} \quad (4)$$

where

M_{ij} is the transition dipole moment from the state i to j;
E_{ij} is the corresponding excitation energy, the subscripts 0, k, and n refer to the ground state S_0, the intermediate state S_k, and the TPA final state S_n, respectively;

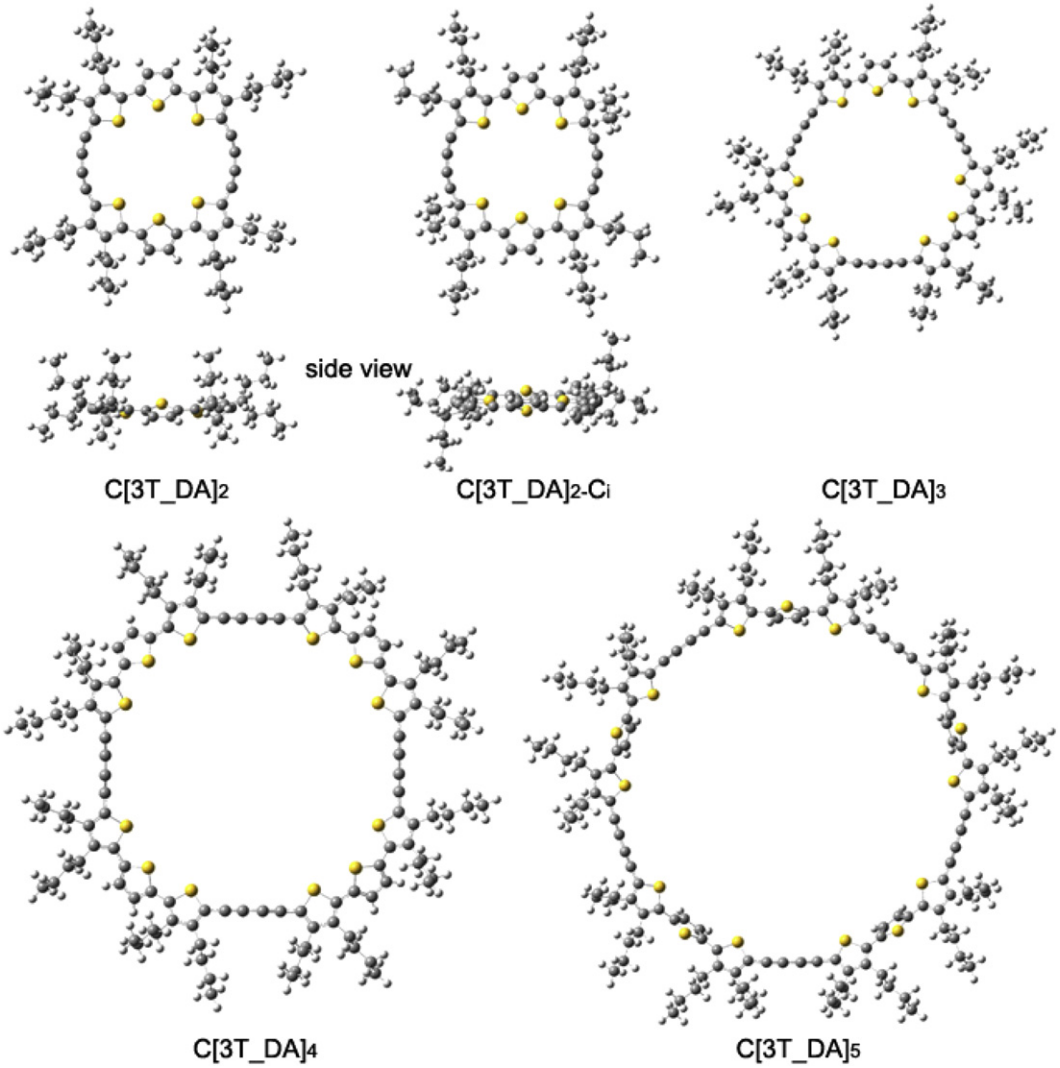

Fig. 2. Optimized geometries of C[3T_DA]$_n$ in gas phase (the side view of C[3T_DA]$_2$ and C[3T_DA]$_2$–C$_i$ are shown).

Table 1
One-photon maximum absorption and transition nature for C[3T_DA]$_n$ compounds by ZINDO method and some experimental data.

Molecule	$\lambda^{(1)}_{max}$/nm		f	Transition nature
C[3T_DA]$_2$	409.4	378.4[a]	0.963	$S_0 \rightarrow S_4$
	392.5	401.0[a]	1.649	$S_0 \rightarrow S_5$
	399.9[b]		0.788[b]	
	386.9[b]		1.284[b]	
	400 [24,26,27]			
C[3T_DA]$_3$	421.4	433.5[a]	2.392	$S_0 \rightarrow S_2$
	421.4	433.5[a]	2.392	$S_0 \rightarrow S_3$
	422 [26,27]			
C[3T_DA]$_4$	452.1	447.8[a]	3.011	$S_0 \rightarrow S_2$
	452.1	447.8[a]	3.011	$S_0 \rightarrow S_3$
	433.4[b]		2.961[b]	
	419.1[b]		2.883[b]	
	420 [26,27]			
C[3T_DA]$_5$	464.0	458.1[a]	3.592	$S_0 \rightarrow S_2$
	464.0	458.1[a]	3.592	$S_0 \rightarrow S_3$
	433 [24,26,27]			

[a] Calculated by TDDFT method.
[b] Calculated values for molecules with C_i symmetry.

M_{0n} is the transition dipole moment from S_0 to S_n.

In principle, any kind of self-consistent field molecular orbital procedure combined with configuration interaction can be used to calculate the physical values in the above expression. In this paper, MPW1B95 functional [32,33] based on the modified Perdew and Wang 1991 exchange functional [34] (mPW or MPW) and Becke's 1995 meta correlation functional [35] (B95), in combination with the standard 6-31G (D) basis set was primarily used to calculate molecular equilibrium geometry using the Gaussian 03 program package [36]. Then, the property of electronic excited states was obtained by single and double electron excitation configuration interaction (SDCI) using ZINDO program [37]. It is well known that the original ZINDO algorithm by Zerner has been adapted only to single-CI, but one has to consider a double excitation configuration for correct determination of the third-order polarizability γ and two-photon absorption spectra. Therefore, we added the double excitation configuration in ZINDO and restricted the CI-active spaces to the five highest occupied and five lowest unoccupied π-orbitals [38]. Then, a program (FTRNLO) compiled by our group is used to calculate the second hyperpolarizability γ and the TPA cross-section according to Eq. (1)–(3). Before that, the ground state OPA spectra, transition dipole moment and the corresponding transition energy are predicted for the TPA properties of the studied molecules.

3. Results and discussion

3.1. Geometry optimization

The molecular structures of the studied C[3T_DA]$_n$ ($n = 2$–5) are shown in Fig. 1. One hand, for systematic comparison, we adopt C_n ($n = 2, 3, 4, 5$) symmetry for all the studied complexes, besides, C[3T_DA]$_5$ has C_{5V} symmetry, [25,39] In addition, we also considered the isomerization of C[3T_DA]$_2$ and C[3T_DA]$_4$ with C_i symmetry [40,41]. Furthermore, the ground state geometries have been optimized at the MPW1B95/6-31G* level in gas phase (Fig. 2). The DFT(total)/Energy of C_n and C_i symmetries of C[3T_DA]$_2$ and C[3T_DA]$_4$ are similar (C[3T_DA]$_2$ and C[3T_DA]$_4$: −4872.4859 and −9745.0508 Hartree for C_n symmetry; −4872.4868 and −9744.7093 Hartree for C_i symmetry, respectively), indicating the isomer of C[3T_DA]$_4$ with C_4 symmetry is more stable than that with C_i symmetry. The energy of isomer of C[3T_DA]$_2$ with C_2 symmetry is slight higher than one with C_i symmetry. Take the side view of C[3T_DA]$_2$ and C[3T_DA]$_2$-C_i as an example (Fig. 2), both the main body skeletons are not coplanar, the arrangement of the middle thiophenes in each unit is different from the other two, turning towards the opposite directions of the plane. While the two butyls on each thiophene for C_n-symmetry molecule distort towards two directions of the plane to counterpoise the whole molecule, but only one pair of butyls in C_i-symmetry molecule seriously deviates from the plane.

As seen from the configurations of the studied molecules, the whole outer annular skeleton is alternating arrangement of single and double bonds. As known from reference [25] bond length alternation (BLA) of the C_n-symmetry molecules, the BLA decreases as the number of thiophene and acetylene unit increases except C[3T_DA]$_5$. It illustrates that the larger the ring is, the more similar the single and double carbon-carbon bond lengths will be, namely, the conjugation of the whole ring gets well. However, the BLA of C[3T_DA]$_5$ gets bigger because of the middle thiophenes distort upwards seriously. In a word, though the butyls distort seriously, the conjugation of the macrocyclic skeleton remains remarkable. It may be owing to the enhancement of molecular coplanarity from introduction of the acetylene group between the two sets of trithiophene units. To some extent, the reducing of BLA may decrease the band gap effectively and increase the π-conjugated effect. It is

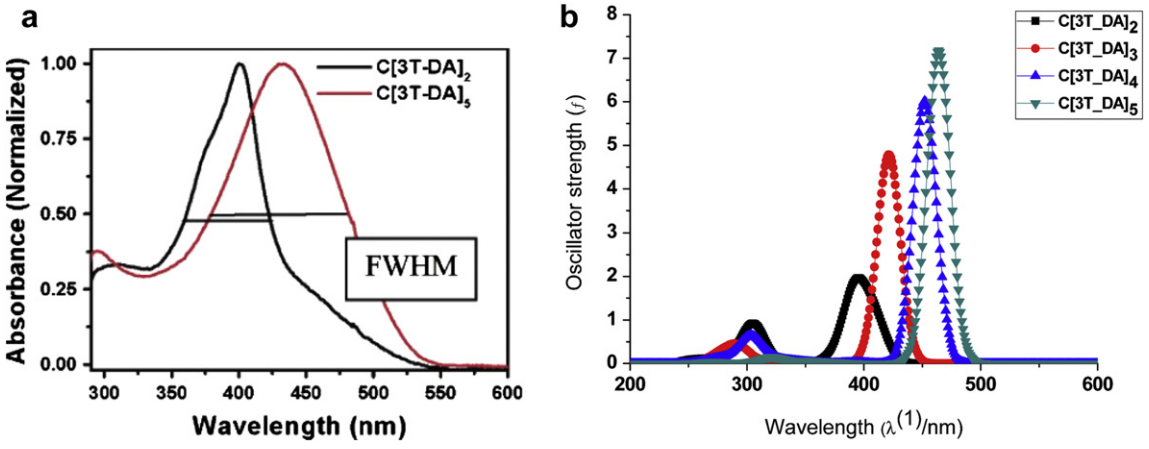

Fig. 3. (a) Experimental absorption spectra of C[3T_DA]$_2$ and C[3T_DA]$_5$ from the reference [24]. (b) Simulated absorption spectra of C[3T_DA]$_n$.

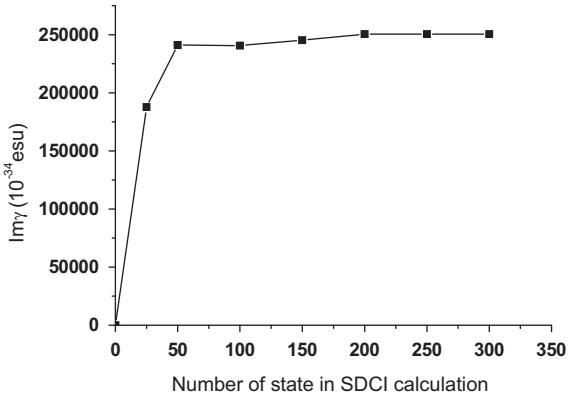

Fig. 4. Dependence of the imaginary part of γ on state number for C[3T_DA]$_5$.

implied that the π-conjugated effect can be further enhanced by enlarging the molecular dimension.

3.2. One-photon absorption property of C[3T_DA]$_n$

The OPA properties of the studied molecules have been calculated by employing TD MPW1B95/6-31G* and ZINDO methods on the basis of the optimized geometries obtained by MPW1B95/6-31G* method in the gas phase [25]. The OPA maximum wavelengths ($\lambda^{(1)}_{max}$), corresponding oscillator strengths (f) and transition nature are listed in Table 1. Both the values of $\lambda^{(1)}_{max}$ calculated by ZINDO and TDDFT methods are in agreement with the experimental values [24,27]. Therefore, OPA properties of all studied molecules calculated using ZINDO method will be discussed in the following discussion.

The absorption curves of C[3T_DA]$_2$ and C[3T_DA]$_5$ have already been observed in experiment (Fig. 3(a)) [24]. As pictured in Fig. 3(a), there are weak absorption peaks around 300 nm, and strong ones at 400–433 nm, respectively. Furthermore, the calculated absorption spectra of C[3T_DA]$_n$ with C_n symmetry were simulated by a Gaussian-type curve and shown in Fig. 3(b). The absorption spectra all have two bands of a weak one and an intense one, which agree with the experimental results. And the intense one slightly enlarges with increasing the number of the C[3T_DA] unit. While C[3T_DA]$_3$, C[3T_DA]$_4$ and C[3T_DA]$_5$ all have two degenerate states, i.e. the second and the third excited states (S_2 and S_3). And the corresponding f obviously increases as the unit number increases. On the other hand, both $\lambda^{(1)}_{max}$ and f of C[3T_DA]$_2$ and C[3T_DA]$_4$ with C_i symmetry are little smaller than that with C_n symmetry, however, the same changing trend of $\lambda^{(1)}_{max}$ and f increasing with increasing the unit number is obtained.

3.3. Two-photon absorption

3.3.1. Molecular structure and TPA cross-section

To further understand the TPA spectrum and its connection with molecular properties, we employed the sum-over-states (SOS) approach, which estimate the imaginary part of third-order optical susceptibility (Im γ). Based on the one- and two-photon selection rules and three-state approximation (Eq. (4)), the one- and two-photon transition allowed states for each studied molecule were identified. Namely, the ***k***th excited state with the largest transition

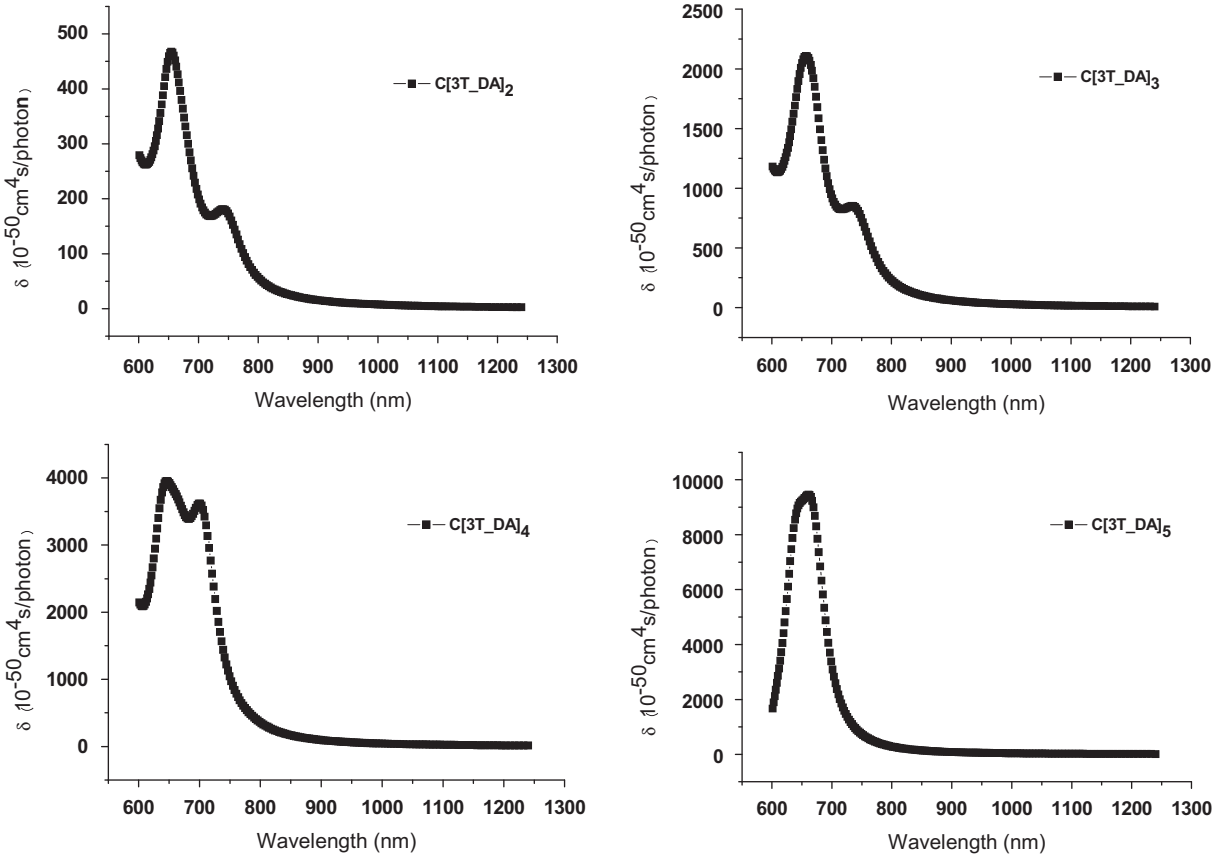

Fig. 5. Two-photon absorption spectra for the studied molecules.

Table 2
TPA properties of C[3T_DA]$_n$ compounds. (1GM = 10^{-50} cm^4 s/photon).

Molecule	$\lambda^{(2)}_{max}$/nm		Transition nature		Im $\gamma/1 \times 10^{-34}$ esu	δ_{max}/GM
C[3T_DA]$_2$	652.6	$S_0 \rightarrow S_{14}$	HOMO → LUMO	14.91%	12 009.4	465.2
			HOMO → LUMO + 3	13.26%		
	650.5[a]					372.2[a]
	760.6				5040.1	143.7
	760.6[a]					110.5[a]
	760 [24]					105 [24]
C[3T_DA]$_3$	667.3	$S_0 \rightarrow S_{13}$	HOMO-3 → LUMO	24.76%	53 536.0	1983.1
			HOMO → LUMO + 3	11.56%		
C[3T_DA]$_4$	640.4	$S_0 \rightarrow S_{21}$	HOMO-4 → LUMO	18.87%	96 072.2	3863.7
			HOMO → LUMO + 3	10.31%		
	656.7[a]					3472.4[a]
C[3T_DA]$_5$	669.5	$S_0 \rightarrow S_{16}$	HOMO-2 → LUMO + 1	15.80%	244 471.2	8997.2
			HOMO-1 → LUMO + 2	15.80%		
			HOMO-4 → LUMO + 3	14.92%		
			HOMO-3 → LUMO + 4	14.92%		
	760.6				20 288.0	578.4
	760 [24]					1470 [24]

[a] Calculated values for molecules with C_i symmetry.

Table 3
The factors of influence on maximum absorptions for C[3T_DA]$_n$. X denotes the value of $\frac{M_{0k}^2 M_{kn}^2}{(E_{0k}-E_{0n}/2)^2 I} + \frac{M_{0n}^2 \Delta\mu_{0n}^2}{(E_{0n}/2)^2 I}$.

Molecule	N_e	$S_0 \rightarrow S_k$	$\boldsymbol{M}_{0k}$/Debye	$\boldsymbol{M}_{kn}$/Debye	$\boldsymbol{M}_{0n}$/Debye	$\boldsymbol{E}_{0k}$/eV	$\boldsymbol{E}_{0n}$/eV	$\Delta\boldsymbol{\mu}_{0n}$	X
C[3T_DA]$_2$	32	$S_0 \rightarrow S_4$	9.149	5.206	0.148	3.028	1.900	−0.019	3750.6
		$S_0 \rightarrow S_5$	11.725	2.956		3.159			1758.6
C[3T_DA]$_3$	48	$S_0 \rightarrow S_2$	14.630	6.737	0.878	2.942	1.858	0.220	17 120.3
		$S_0 \rightarrow S_3$	14.630	6.732		2.942			17 096.9
C[3T_DA]$_4$	64	$S_0 \rightarrow S_2$	17.002	8.434	0.000	2.742	1.936	−0.132	46 647.7
		$S_0 \rightarrow S_3$	17.002	8.434		2.742			46 647.7
C[3T_DA]$_5$	80	$S_0 \rightarrow S_2$	18.812	10.500	0.352	2.672	1.852	0.449	91 403.2
		$S_0 \rightarrow S_3$	18.812	10.500		2.672			91 403.2

moment $\boldsymbol{M}_{0k}$ was regarded as the mediate state and the $\boldsymbol{n}$th state with the largest transition moment $\boldsymbol{M}_{kn}$ as the final state during the TPA calculation. After getting the maximum TPA peak ($\lambda^{(2)}_{max}$), the third-order optical susceptibility ($\langle\langle\gamma\rangle\rangle$) and the TPA cross-section ($\boldsymbol{\delta}_{max}$) were calculated in terms of Eq. (1)–(3) by using FTRNLO program, where 300 states were chosen. In order to ascertain whether 300 states is enough for the convergence of γ, the dependence of the imaginary part of the third-order optical susceptibility (Im γ) on state number for all studied molecules was investigated. The largest molecule C[3T_DA]$_5$ was taken as an example, when the state number accumulated to 200 states, Im γ of C[3T_DA]$_5$ has already converged as illustrated in Fig. 4. Moreover, other molecules were studied in the same way, and the results show that all the Im γ are converged before 300 states.

It is well known that the TPA wavelength at near infrared region (NIR) is useful in the practical application such as biological vivo image, photodynamic therapy and so on [42]. In experiment, the TPA cross-section values of two studied molecules were measured at 760 nm. Thus, TPA peaks were calculated by point scanning in the wavelength range of 600–1240 nm, and the results were plotted in Fig. 5. The obtained details of TPA properties together with available experimental values are listed in Table 2. As shown in Fig. 5 and Table 2 that all the studied molecules have a strong two-photon absorption between 640 and 670 nm, and they also have a weak one around 740 nm except C[3T_DA]$_5$, because of the C_{5V} symmetry of C[3T_DA]$_5$ is different from other molecules. While the TPA cross-section of C[3T_DA]$_n$ enhances with increasing the unit number. So alternately adding moieties of the thiophene and acetylene into the ring can enlarge its TPA cross-section. When five thiophene and acetylene units are incorporated to form C[3T_DA]$_5$, the $\boldsymbol{\delta}_{max}$ increases to 8997.2GM, which is about 18 times larger than that of C[3T_DA]$_2$ (465.2GM). Therefore, the number of thiophene and acetylene units significantly affects the TPA cross-section value. In short, the effective extension of the π-conjugation and increase of π-electron number are essentially significant for the increase of TPA cross-section. Furthermore, TPA wavelength and cross-section of C[3T_DA]$_2$ and C[3T_DA]$_4$ with C_i symmetry are calculated and listed in Table 2. The results suggest that the sites of $\lambda^{(2)}_{max}$ are close to that of C_n symmetry, and the $\boldsymbol{\delta}_{max}$ also enlarges with increasing the unit number, but the values are little smaller than that of the C_n symmetry.

In order to clarify the increase of $\boldsymbol{\delta}_{max}$, according to Eq. (4) the internal influences on $\boldsymbol{\delta}_{max}$ were analyzed. During the calculation, $\boldsymbol{\delta}_{max}$ is proportional to the square product of $\boldsymbol{M}_{0k}$ and $\boldsymbol{M}_{kn}$, and inversely proportional to the square of the energy detuning term ($\boldsymbol{E}_{0k} - \boldsymbol{E}_{0n}/2$). As summarized in Table 3, both $\boldsymbol{M}_{0k}$ and $\boldsymbol{M}_{kn}$ increase

Table 4
The oscillator strengths corresponding to maximum absorptions of C[3T_DA]$_n$.

Molecule	C[3T_DA]$_2$		C[3T_DA]$_3$		C[3T_DA]$_4$		C[3T_DA]$_5$	
	$S_0 \rightarrow S_4$	$S_0 \rightarrow S_5$	$S_0 \rightarrow S_2$	$S_0 \rightarrow S_3$	$S_0 \rightarrow S_2$	$S_0 \rightarrow S_3$	$S_0 \rightarrow S_2$	$S_0 \rightarrow S_3$
f_{0k}	0.963	1.649	2.392	2.392	3.011	3.011	3.592	3.592
f_{kn}	0.080	0.021	0.133	0.132	0.304	0.304	0.434	0.434
$f_{0k} \times f_{kn}$	0.077	0.035	0.318	0.316	0.915	0.915	1.559	1.559

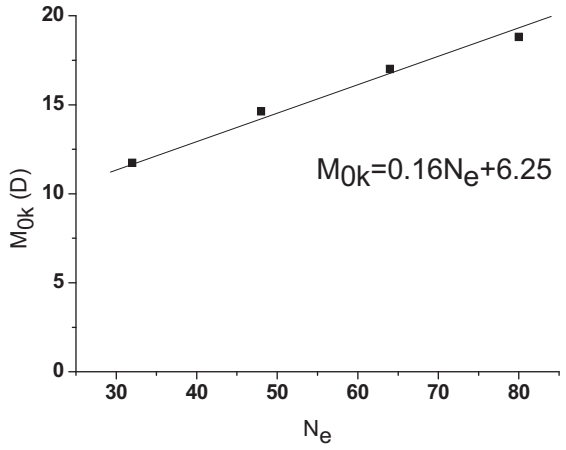

Fig. 6. The dependence of $\boldsymbol{M}_{0k}$ with N_e.

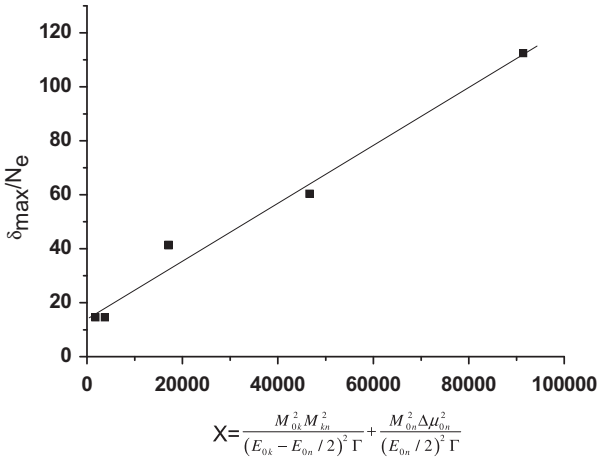

Fig. 8. The relation between the δ_{max}/N_e and factors of C[3T_DA]$_n$ molecules.

with increasing the unit number. At the same time, $\boldsymbol{E}_{0k}$ decreases and $\boldsymbol{E}_{0n}$ increases mostly, so that $(\boldsymbol{E}_{0k} - \boldsymbol{E}_{0n}/2)$ decreases. The combination of these effects leads to a significant increase of $\boldsymbol{\delta}_{max}$. During the calculation of $X(=\boldsymbol{M}_{0k}{}^2\boldsymbol{M}_{kn}{}^2/(\boldsymbol{E}_{0k} - \boldsymbol{E}_{0n}/2)^2\Gamma + \boldsymbol{M}_{0n}{}^2\ \Delta\ \boldsymbol{\mu}_{0n}{}^2/(\boldsymbol{E}_{0n}/2)^2\Gamma)$, $\boldsymbol{M}_{0k}$ and $\boldsymbol{M}_{kn}$ have more important influence on the results. That is to say, $\boldsymbol{M}_{0k}$ and $\boldsymbol{M}_{kn}$ dominate the changing of $\boldsymbol{\delta}_{max}$.

Except for these factors mentioned in Eq. (4), it can also be found from Table 4 that both of the oscillator strengths from ground state to mediate state (f_{0k}) and from mediate state to final state (f_{kn}) increase with increasing of the unit number. Moreover, there is direct proportion relation between $\boldsymbol{\delta}_{max}$ and $f_{0k} \times f_{kn}$. That is, oscillator strength would play an important part in the enlargement of the TPA cross-section.

As mentioned before, the feature of the whole outer ring of the studied molecules is constituted by alternating single and double carbon-carbon bonds, which exhibited a successive π-bond, and each carbon-carbon double bond have two π-electrons. The important transition moments $\boldsymbol{M}_{0k}$ are related to the charge redistribution, which may be expected to be in proportion to the length of a linear chromophore or the number of π-electrons (N_e), so the dependence of $\boldsymbol{M}_{0k}$ on N_e is drawn, giving $\boldsymbol{M}_{0k} \propto N_e$ (Fig. 6). It shows a good linear relationship, which can be fitted as $\boldsymbol{M}_{0k} = 0.16N_e + 6.25$. So if N_e is known, the $\boldsymbol{M}_{0k}$ of this series of C[3T_DA]$_n$ can be estimated roughly. Also as N_e increases from C[3T_DA]$_2$ to C[3T_DA]$_5$, the relationship between $\boldsymbol{\delta}_{max}$ and N_e is described in Fig. 7, showing $\boldsymbol{\delta}_{max}$ increases gradually with N_e increasing. Moreover, as observed in Table 3, it is surprised to find that the dependence of X on N_e can be described as the formula $X \approx (\delta^0_{max}/N_e) \times 3N_\pi \times m(m+2)$, in which $\delta^0_{max}/N_e = 3750.6/32$ denotes the basic TPA cross-section value, N_π denotes the basic π-electron number of each unit, where it is 16, and $m = n - 2$, $(n = 3–5)$. So that it can be abbreviated as $X \approx 5625.9 \times n(n-2)$, when $n = 2$, it follows $X \approx (\delta^0_{max}/N_e) \times 3N_\pi \times 2$. This empirical trend indicates that the degree of $\boldsymbol{\delta}_{max}$ can be predicted and its approximate X value can be estimated when the n of C[3T_DA]$_n$ compounds is known. So it provides a new way for the prediction of the TPA cross-section when the molecular dimension enlarges.

So as to discuss the average TPA cross-section over the whole π-conjugated ring, the relation between δ^0_{max}/N_e and X is depicted in Fig. 8. The calculated points are well-distributed at two sides of the fitting line, which shows a proportional relationship between $\boldsymbol{\delta}_{max}/N_e$ and X. It indicates three-state approximation value X can predict the changing trend of $\boldsymbol{\delta}_{max}$ in general.

Combining the known increasing trend of $\boldsymbol{\delta}_{max}$ and the calculated static second-order nonlinear optical coefficients β_0 of C[3T_DA]$_n$ $(n = 2–5)$ $(-6.88, -17.43, -49.24, -90.52 \times 10^{-30}$ esu) in another report [25], whose absolute value also increases with increasing the C[3T_DA] unit number. So the relation between $\boldsymbol{\delta}_{max}$ and the absolute value of β_0 have been described in Fig. 9. It is

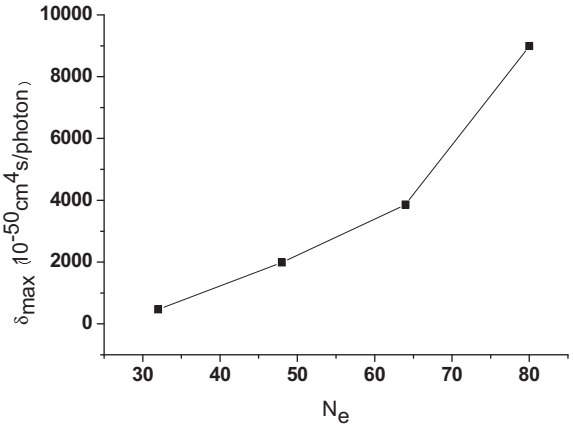

Fig. 7. The dependence of $\boldsymbol{\delta}_{max}$ with N_e.

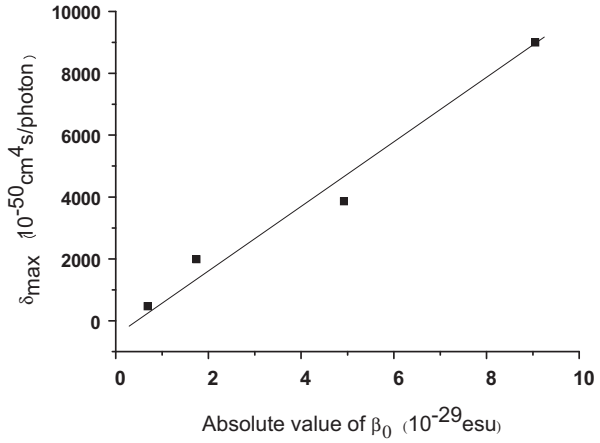

Fig. 9. The relation between $\boldsymbol{\delta}_{max}$ and β_0.

demonstrated there is an approximately proportional relation between them. That is to say, δ_{max} increases with increasing the absolute value of β_0.

3.3.2. Electronic structure

In order to further understand how the molecular structure affects the frontier molecular orbitals and ascertain the internal factors which can influence TPA properties, the frontier molecular orbitals related to the important transition in TPA process are drawn in Fig. 10. It is easy to find that all the electron densities locate on the peripheral C–C π-electron delocalization circuit, but none on the ambient butyl. The electron clouds located on the occupied orbitals distribute on carbon-carbon double and triple bonds from thiophenes and acetylenes, and the electron clouds located on the unoccupied orbitals distribute on carbon-carbon single bonds. And there is no electron cloud distribution on sulfur in all occupied orbitals, showing the sulfur atoms did not take part in the conjugation over the whole ring skeleton.

Combining Table 2, the characterization of orbital transition related to TPA was analyzed. During HOMO → LUMO transition of C[3T_DA]$_2$, the change of electronic clouds is unobvious, but it is obvious on the two acetylenes during HOMO → LUMO + 3 transition. With regard to the molecule C[3T_DA]$_3$, the intermolecular charges slightly transfer from the whole ring to the thiophenes. During HOMO-4 → LUMO transition of C[3T_DA]$_4$, the charges transfer to the two acetylenes, and its distribution is the same as that of C[3T_DA]$_2$, but stronger. As to C[3T_DA]$_5$, there are four main transitions. During HOMO-2 → LUMO + 1 and HOMO-1 → LUMO + 2 transitions, the charges transfer to the middle thiophenes and concentrate in three units. But for HOMO-4 → LUMO + 3 and HOMO-3 → LUMO + 4 transitions, the locations of electron clouds change greatly, intramolecular charges transfer to their complementary position (Fig. 10). It illustrates that the π-conjugated effect strengthens and intramolecular charge transfer (ICT) gets stronger with increasing the number of C[3T_DA] unit, furthermore, larger δ_{max} are obtained. And the thiophene and acetylene unit in each compound plays a role of

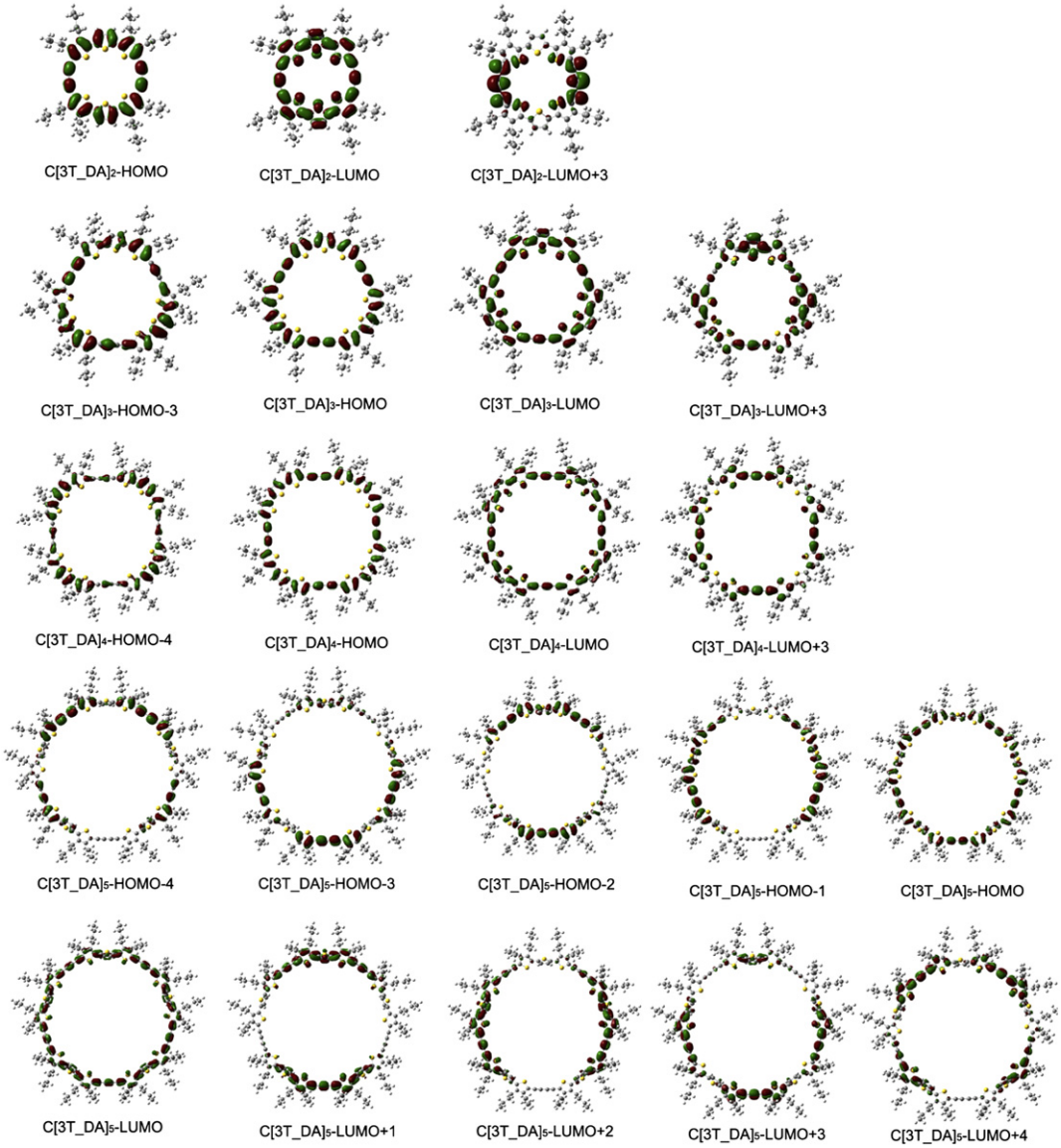

Fig. 10. Contour surfaces of the frontier orbitals for C[3T_DA]$_n$.

equal importance in the increase of δ_{max}. In a word, the larger the number of molecular unit is, the higher the conjugation is, as a result, the larger the two-photon absorption cross-section will be obtained.

4. Conclusion

The one- and two-photon absorption spectra, TPA transitions and TPA cross-sections of compounds C[3T_DA]$_n$ ($n = 2-5$) have been explored in detail using DFT combing with ZINDO and FTRNLO programs. And the influence of some factors on OPA and TPA properties was analyzed. The presented results allow us to conclude that the one-photon absorption $\lambda^{(1)}{}_{max}$ of macrocyclic thiophene derivatives are transparent ranging from 390 to 470 nm, and two-photon absorption $\lambda^{(2)}{}_{max}$ locate in IR range from 640 to 670 nm. The two absorptions are located at different windows, and don't superpose with each other. Therefore, C[3T_DA]$_5$ et al. macrocyclic thiophene molecules will have a potential application in the TPA dynamic therapy. Both $\lambda^{(1)}{}_{max}$ and $\lambda^{(2)}{}_{max}$ of C[3T_DA]$_n$ enlarge as the number of the C[3T_DA] unit increases no matter what symmetry is. The series of compounds C[3T_DA]$_n$ with C_n symmetry exhibit larger δ_{max} in IR range. The δ_{max} of C[3T_DA]$_5$ (8997.2GM) is about 18 times larger than that of C[3T_DA]$_2$, which is resulted from the enlargement of the π-conjugated extent and the reinforcement of ICT. And the unit of thiophene and acetylene in each compound also has important contribution to the increase of δ_{max}. $\boldsymbol{M}_{0k}$, $\boldsymbol{M}_{kn}$ and N_e all play important roles on δ_{max}. Moreover, an approximated formulation of δ_{max} is concluded as $X \approx (\delta^0_{max}/N_e) \times 3N_\pi \times n(n-2)$, by which the X of bigger macrocyclic thiophene derivatives C[3T_DA]$_n$ can be derived. Besides, both $f_{0k} \times f_{kn}$ and β_0 are proportional to δ_{max}. In summary, the present computational results offer a new design strategy to enhance molecular TPA cross-section through enlarging the macrocyclic dimension. All above suggest this series of macrocyclic thiophene derivatives are expected to be useful two-photon materials.

Acknowledgement

This work is supported by the Natural Science Foundation of China (No. 20973078 and 20673045), special funding to basic scientific research projects for Central Colleges as well as the Open Project of the State Key Laboratory for Superamolecular Structure and Material of Jilin University (SKLSSM200716).

References

[1] Kanis DR, Ratner MA, Marks TJ. Design and construction of molecular assemblies with large second-order optical nonlinearities. Quantum chemical aspects. Chemical Reviews 1994;94:195–242.
[2] Boni LD, Andrade AA, Corrêa DS, Balogh DT, Zilio SC, Misoguti L, et al. Nonlinear absorption spectrum in MEH-PPV/chloroform solution: a competition between two-photon and saturated absorption processes. Journal of Physical Chemistry B 2004;108:5221–4.
[3] Margineanu A, Hofkens J, Cotlet M, Habuchi S, Stefan A, Qu JQ, et al. Photophysics of a water-soluble Rylene dye: comparison with other fluorescent molecules for biological applications. Journal of Physical Chemistry B 2004; 108:12242–51.
[4] Göeppert-Mayer M. Über elementaraktemit zwei quantensprungen. Annals of Physics 1931;9:273–95.
[5] Denk W, Strickler JH, Webb WW. Two-photon laser scanning fluorescence microscopy. Science 1990;248:73–6.
[6] Arnbjerg J, Jimenez-Banzo A, Paterson MJ, Nonell S, Borrell JI, Christiansen O, et al. Two-Photon absorption in tetraphenylporphycenes: are porphycenes better candidates than porphyrins for providing optimal optical properties for two-photon photodynamic therapy? Journal of American Chemistry Society 2007;129:5188–99.
[7] Lin TC, He GS, Zheng Q, Prasad PN. Degenerate two-/three-photon absorption and optical power-limiting properties in femtosecond regime of a multibranched chromophore. Journal of Material Chemistry 2006;16:2490–8.
[8] Maruo S, Nakamura O, Kawata S. Three-dimensional microfabrication with two-photon-absorbed photopolymerization. Optics Letters 1997;22:132–4.
[9] Parthenopoulos DA, Rentzepis PM. Three-dimensional optical storage memory. Science 1989;245:843–5.
[10] He GS, Zhao CF, Bhawalkar JD, Prasad PN. Two-photon pumped cavity lasing in novel dye doped bulk matrix rods. Applied Physics Letters 1995;67: 3703–5.
[11] Zhao CF, He GS, Bhawalkar JD, Park CK, Prasad PN. Newly synthesized dyes and their polymer/glass composites for one- and two-photon pumped solid-state cavity lasing. Chemistry of Materials 1995;7:1979–83.
[12] Wang Y, He GS, Prasad PN, Goodson III T. Ultrafast dynamics in multibranched structures with enhanced two-photon absorption. Journal of American Chemistry Society 2005;127:10128–9.
[13] Zhou X, Ren AM, Feng JK, Liu XJ. Theoretical study of two-photon absorption properties of a series of double-layer paracyclophane derivatives. Journal of Physical Chemistry A 2003;107:1850–8.
[14] Zhao Y, Ren AM, Feng JK, Sun CC. Theoretical study of one-photon and two-photon absorption properties of perylene tetracarboxylic derivatives. Journal of Chemical Physics 2008;129:014301.
[15] Leng WN, Bazan GC, Kelley AM. Solvent effects on resonance Raman and hyper-Raman scatterings for a centrosymmetric distyrylbenzene and relationship to two-photon absorption. Journal of Chemical Physics 2009;130: 044501.
[16] Li X, Zhao YX, Wang T, Shi MQ, Wu FP. Coumarin derivatives with enhanced two-photon absorption cross-sections. Dyes and Pigments 2007;74:108–12.
[17] Abbotto A, Beverina L, Bozio R, Facchetti A, Ferrante C, Pagani GA, et al. Novel heteroaromatic-based multi-branched dyes with enhanced two-photon absorption activity. Chemical Communication 2003;7:2144–5.
[18] Fakis M, Fitilis I, Stefanatos S, Vellis P, Mikroyannidis J, Giannetas V, et al. The photophysics and two-photon absorption of a series of quadrupolar and tribranched molecules: the role of the edge substituent. Dyes and Pigments 2009;81:63–8.
[19] Moore JS, Zhang J. Efficient synthesis of nanoscale macrocyclic hydrocarbons. Angewandte Chemie International Edition 1992;31:922–4.
[20] Bednarz M, Reineker P, Mena-Osteritz E, Baeuerle P. Optical absorption spectra of linear and cyclic thiophenes—selection rules manifestation. Journal of Luminescence 2004;110:225–31.
[21] Williams-Harry M, Bhaskar A, Ramakrishna G, Goodson III T, Imamura M, Mawatari A, et al. Giant thienylene-acetylene-ethylene macrocycles with large two-photon absorption cross section and semishape-persistence. Journal of American Chemistry Society 2008;130:3252–3.
[22] Kiriy N, Bocharova V, Kiriy A, Stamm M, Krebs FC, Adler HJ. Designing thiophene-based azomethine oligomers with tailored properties: self-assembly and charge carrier mobility. Chemistry of Materials 2004;16:4765–71.
[23] Nishida J, Miyagawa T, Yamashita Y. Novel thiophene oligomers containing a redox active hexaarylethane unit. Organic Letters 2004;6:2523–6.
[24] Bhaskar A, Ramakrishna G, Hagedorn K, Varnavski O, Osteritz EM, Baluerle P, et al. Enhancement of two-photon absorption cross-section in macrocyclic thiophenes with cavities in the nanometer regime. Journal of Physical Chemistry B 2007;111:946–54.
[25] Huang S, Ren AM, Zou LY, Zhao Y, Guo JF, Feng JK. Computational study of the electronic structures, UV–Vis spectra and static second-order nonlinear optical susceptibilities of macrocyclic thiophene derivatives. submitted for publication.
[26] Casadoa J, Zgierski MZ, Fuhrmann G, Juan PB, Navarreteb JTL. Structural implications of ring shape, dimension, and metal atom insertion in nanosized cyclic oligothiophenes: joint Raman and density functional theory study. Journal of Chemical Physics 2006;125:044518.
[27] Fuhrmann GL. Synthesis and characterization of oligothiophene – based fully π-conjugated macrocycles the department of organic chemistry II. Germany: University of Ulm; 2006.
[28] Kogej T, Beljonne D, Meyers F, Perry JW, Marder SR, Brédas JL. Mechanisms for enhancement of two-photon absorption in donor–acceptor conjugated chromophores. Chemical Physics Letters 1998;298:1–6.
[29] Orr BJ, Ward JF. Perturbation theory of the non-linear optical polarization of an isolated system. Molecular Physics 1971;20:513–26.
[30] Bishop DM, Luis JM, Kirtman B. Vibration and two-photon absorption. Journal of Chemical Physics 2002;116:9729–39.
[31] Beljonne D, Wenseleers W, Zojer E, Shuai Z, Vogel H, Pond SJK, et al. Role of dimensionality on the two-photon absorption response of conjugated molecules: the case of octupolar compounds. Advanced Functional Materials 2002; 12:631–41.
[32] Zhao Y, Truhlar DG. Hybrid meta density functional theory methods for thermochemistry, thermochemical kinetics, and noncovalent interactions: the MPW1B95 and MPWB1K models and comparative assessments for hydrogen bonding and van der waals interactions. Journal of Physical Chemistry A 2004; 108:6908–18.
[33] Zhao Y, Truhlar DG. Benchmark databases for nonbonded interactions and their use to test density functional theory. Journal of Chemical Theory and Computation 2005;1:415–32.
[34] Perdew JP. In: Ziesche P, Eschig H, editors. Electronic structure of solids '91. Berlin: Akademie Verlag; 1991. p. p11.
[35] Becke AD. Density-functional thermochemistry. IV. A new dynamical correlation functional and implications for exact-exchange mixing. Journal of Chemical Physics 1996;104:1040–6.

[36] Frisch MJ, Trucks GW, Schlegel HB, Scuseria GE, Robb MA, Cheeseman JR, et al. Gaussian 03 (Revision D02). Pittsburgh, PA: Gaussian Inc.; 2003.
[37] Anderson WP, Edwards WD, Zerner MC. Calculated spectra of hydrated ions of the first transition-metal series. Inorganic Chemistry 1986;25:2728–32.
[38] Zhang XB, Feng JK, Ren AM, Sun CC. Theoretical study of two-photon absorption properties of a series of ferrocene-based chromophores. Journal of Physical Chemistry A 2006;110:12222–30.
[39] Huang S, Ren AM, Li Z, Zhao Y, Min CG. Theoretical study on structures and UV–Vis spectra of macrocyclic thiophene derivatives. Chemical Journal of Chinese Universities 2010;3:553–8.
[40] Fuhrmann G, Debaerdemaeker T, Bäuerle P. C–C bond formation through oxidatively induced elimination of platinum complexes—a novel approach towards conjugated macrocycles. Chemical Communications; 2003:948–9.
[41] Kromer J, Rios-Carreras I, Fuhrmann G, Musch C, Wunderlin M, Debaerdemaeker T, et al. Synthesis of the first fully alpha-conjugated macrocyclic oligothiophenes cyclo [n] thiophenes with tunable cavities in the nanometer regime. Angewandte Chemie-International Edition 2000;39:3481–6.
[42] Hilderbrand SA, Weissleder R. Near-infrared fluorescence: application to in vivo molecular imaging. Current Opinion in Chemical Biology 2010;14:71–9.